Room Temperature Pseudo-Solid State Iron Fluoride Conversion Battery with High Ionic Conductivity and Low Interfacial Resistance

*Aliya S. Lapp,[1] Laura C. Merrill,[2] Bryan R. Wygant,[3] David S. Ashby,[1] Austin S. Bhandarkar,[1] Alan C. Zhang,[1] Elliot J. Fuller,[1] Katharine L. Harrison,[2] Timothy N. Lambert,[3] and A. Alec Talin.[1,]**

[1]Sandia National Laboratories, Materials Physics Department, 7011 East Avenue, Livermore, CA, 94550, USA.

[2]Sandia National Laboratories, Nanoscale Sciences Department, 1515 Eubank Blvd. SE, Albuquerque, NM, 87123, USA.

[3]Sandia National Laboratories, Photovoltaics and Materials Technology Department, 1515 Eubank Blvd. SE, Albuquerque, NM, 87123, USA.

*To whom correspondence should be addressed.

Email: aatalin@sandia.gov

Submitted: 6 September, 2022

Revised:

Keywords: batteries, pseudo-solid state, gel polymer electrolytes, localized high concentration electrolytes, iron fluoride, conversion, ionogels

Abstract

Li metal batteries (LMBs) employing conversion cathode materials (e.g., FeF_3) are a promising way to prepare inexpensive, environmentally friendly batteries with high energy density. Pseudo-solid state ionogel separators harness the energy density and safety advantages of solid state LMBs, while alleviating key drawbacks (e.g., poor ionic conductivity and high interfacial resistance). In this work, a pseudo-solid state conversion battery (Li-FeF_3) is presented that achieves stable, high rate (1.0 mA cm^{-2}) cycling at room temperature. The batteries described herein contain gel-infiltrated FeF_3 cathodes prepared by exchanging the ionic liquid in a polymer ionogel with a localized high concentration electrolyte (LHCE). The LHCE gel merges the benefits of a flexible separator (e.g., adaptation to conversion-related volume changes) with the excellent chemical stability and high ionic conductivity (~2 mS cm^{-1} at 25°C) of an LHCE. The latter property is in contrast to previous solid state iron fluoride batteries, where poor ionic conductivities necessitated elevated temperatures to realize practical power levels. The stable, room temperature Li-FeF_3 cycling performance obtained with the LHCE gel at high current densities paves the way for exploring a range of architectures including flexible, three-dimensional, and custom shape batteries.

Introduction

High energy density batteries are needed to meet ever expanding energy demands. Li metal batteries (LMBs) containing conversion cathode materials are a promising route for achieving this goal due to large working voltages,[1, 2] multi-electron reactions,[1, 2] and the exceptional theoretical capacity of Li metal (3860 mAh g^{-1}).[3, 4] For example, the three-electron reaction that FeF_3 undergoes with Li,[1] paired with a 2.7 V Li-FeF_3 potential difference,[2] confers a theoretical energy density of 1922 Wh kg^{-1}.[1] High energy density, along with environmental

benignity and rich natural abundance, has spurred interest in FeF_3 as an LMB cathode material.[1, 2, 5-7]

Despite these advantages, Li metal introduces safety concerns (e.g., flammability, side reactions, and dendrites) that are exacerbated by liquid electrolytes.[3, 8] Accordingly, there has been a push towards solid state batteries.[3, 9] The biggest challenges encountered with solid state batteries are low ionic conductivities, difficulty forming intimate low resistance interfaces with microporous electrodes, and mechanical instability introduced by electrode volumetric changes.[9, 10] An innovative way to address these detriments is to use a pseudo-solid state ionogel (IG) separator.[11, 12]

IGs consist of an ionic liquid electrolyte (ILE) encapsulated by a solid matrix.[11, 12] The coexistence of solid and liquid phases combines the mechanical properties of a solid (e.g., structural support and elasticity) with the physical properties of a liquid electrolyte (*vide infra*).[11-13] ILEs have high ionic conductivities and are stable over a broad range of temperatures, chemical environments, and voltages.[11-13] Additionally, ILEs are non-flammable[11-13] and can thus improve the safety of LMBs. When an IG is deposited onto a cathode, the low volatility of the ILE assists in forming a gel that penetrates the pores of the cathode. [11, 13] In turn, this provides a localized electrolyte reservoir that decreases interfacial resistance relative to pure solid-state electrolytes. [11, 13]

We recently reported a procedure for exchanging the ILE in an IG (through a series of passive diffusion steps) with a less viscous electrolyte.[14] This procedure can be used to impart the gel with more desirable properties (e.g., lower charge transfer resistance and higher conductivity).[14] In the present report, exchange of the ILE in a flexible, polymer IG with a localized high concentration electrolyte (LHCE; *vide infra*) imbues high ionic conductivity, high coulombic efficiency (CE), and stability with both electrodes (cathode and anode), while preserving pore interpenetration from the original IG. The latter property represents a marked

advantage relative to freestanding polymer gels prepared by swelling, [12, 15] as it leads to the formation of intimate and mechanically compliant electrode/electrolyte interfaces.

LHCEs are a subset of highly concentrated electrolytes (HCEs), which are distinguished by their inherent lack of free solvent molecules.[8, 16, 17] The ubiquity of coordinated solvent molecules in HCEs inhibits the electrolyte from participating in side reactions.[8, 16, 17] For example, it has previously been shown that the use of LiFSI-based HCEs in iron fluoride batteries leads to a stable passivation layer that hinders active material dissolution,[5, 18] ion leaching,[18] and Li dendrites.[17]

LHCEs are formed by diluting an HCE with a component that has little to no solubility with the electrolyte salt (e.g., a diluent). In this way, LHCEs retain the beneficial solvent structure of HCEs, while diminishing their drawbacks (e.g., high viscosity/cost and inferior wetting properties). [8, 16, 17] Recently, our group showed that the particular LHCE used in the present report (*vide infra*) is stable with both Li metal and FeF_3, enabling high CE and rate capability for Li-FeF_3 batteries.[19]

Despite the beneficial properties of FeF_3 (*vide supra*), commercialization of rechargeable Li-FeF_3 batteries has been impeded by low CE,[1, 7] voltage hysteresis,[1, 7, 18] slow kinetics,[1] low electronic conductivity,[1, 6, 18] electrolyte decomposition,[18, 20] and volumetric changes during the conversion reaction.[18, 20] Use of an LHCE can address low CE and electrolyte decomposition. However, a more comprehensive strategy is needed to tackle the remaining challenges.

Yushin and coworkers previously showed that using an elastic separator (a polyethylene oxide (PEO)-based solid polymer electrolyte (SPE)) in Li-FeF_2 batteries alleviated several of the issues above.[20] In particular, separator flexibility during volume expansion stabilized the cathode electrolyte interface, which in turn decreased voltage hysteresis and the maladies of mechanical fatigue (e.g., ion leaching and shortened cycle life).[20]

Subsequent reports of solid state iron fluoride batteries improved on this design (achieving ~150-200 mAh g^{-1} after 1200 cycles at 1 C) by adding various fillers to PEO-based SPEs (e.g., graphitic carbon nitride and a Ce metal organic framework).[21, 22] Despite these gains, previous solid state iron fluoride batteries suffered from two major limitations: (1) low ionic conductivities (maximum of 0.03 mS cm^{-1} at 30°C and 0.31 mS cm^{-1} at 60°C) and (2) low mass loadings (maximum of 0.6-0.8 mg cm^{-2}).[20-22] These properties prevented practical room temperature operation.

Herein, we show that using a thin (~60 μm) gel prepared by electrolyte exchange of the ILE (1.0 M LiFSI in $PYR_{14}TFSI$) in a PVDF-HFP IG with an LHCE (1.0 LiFSI: 1.2 DME: 3.0 TTE, by mole), results in a pseudo-solid state Li-FeF_3 battery with high rate capability at room temperature (up to 1.0 mA cm^{-2}) and stable cycling. Improved performance at room temperature is enabled by three key properties of the LHCE-filled gel. First, ionic conductivity (1.92 mS cm^{-1} at 25°C and 3.74 mS cm^{-1} at 60°C) is up to two orders of magnitude greater than previous solid state iron fluoride batteries (*vide supra*).[20-22] Second, the unique solvent structure of the LHCE results in high CE (>98%) and stabilizes the chemical interface of the gel with both the anode and cathode. Third, the flexibility of the polymer gel enables adaptability to the significant volume expansion that occurs during the conversion reaction (up to 30%).[20] Overall, the results obtained here have the potential to be broadly applicable to batteries employing conversion cathodes. Finally, although we focus on the LHCE-filled gel (due to its superior room temperature performance), we show promising preliminary results for the precursor IG at elevated temperature (60 °C).

Results and Discussion

Characterization of FeF_3 cathodes. Figure S1a shows that the range of FeF_3 particle sizes is ~100-400 nm. Raman spectroscopy (Figure S1b) indicates the presence of just two species: FeF_3 (170, 303, and 437 cm^{-1})[23, 24] and carbon (1350 and 1600 cm^{-1}; D and G bands,

respectively).[25] The lack of additional peaks suggests that the FeF_3 is phase pure. XRD (Figure S1c) supports this claim, with the exception of a minor FeF_2 impurity. Cross-sectional SEM (Figure 1a) of a representative FeF_3 cathode indicates that that the average layer thickness of FeF_3 (mixed with C) is 20 ± 5 μm (Figure 1b; N = 200 thickness measurements of randomly selected cathode regions).

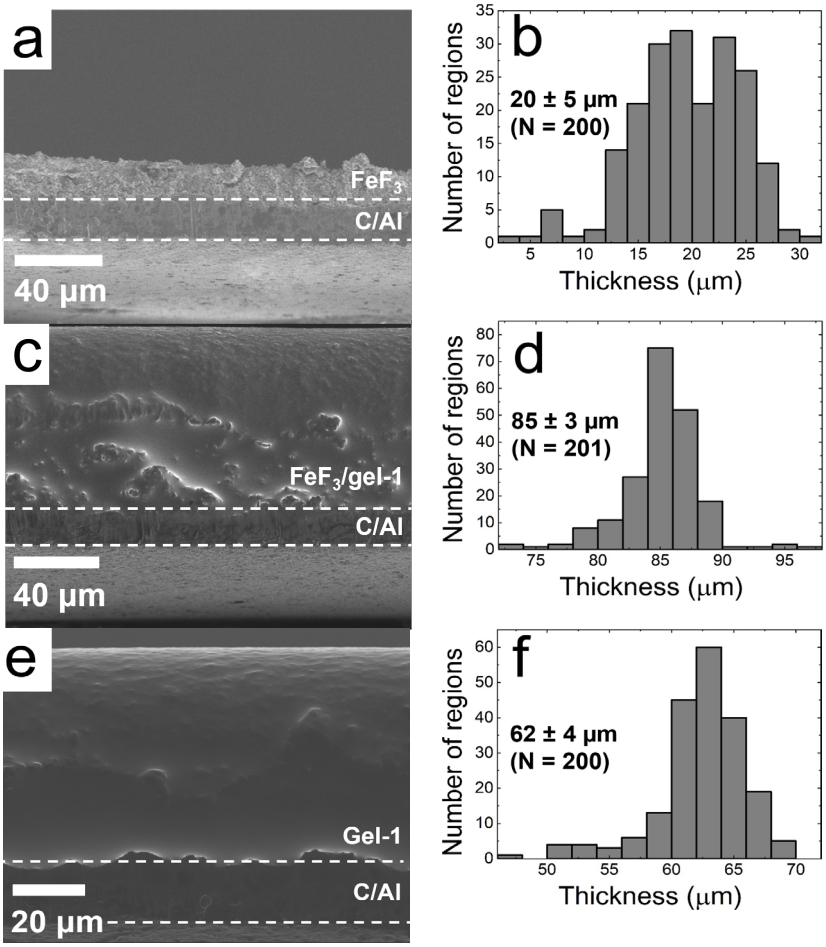

Figure 1. SEM images and thickness distribution histograms for: (a,b) an uncoated FeF_3 cathode, (c,d) FeF_3 coated with gel-1 (= PVDF-HFP filled with 1.0 M LiFSI in $PYR_{14}TFSI$), and (e,f) gel-1 on C-coated Al foil (in the absence of FeF_3). Average thicknesses of the (b) FeF_3, (d) FeF_3/gel-1, and (f) gel-1 layers are indicated in each histogram.

PVDF-HFP gel characterization. We note that two different types of PVDF-HFP gels are discussed in the present report: (1) gel-1, which is filled with ionic liquid electrolyte

(ILE; 1.0 M LiFSI in $PYR_{14}TFSI$) and (2) gel-2, filled with a localized high concentration electrolyte (LHCE; 1.0 LiFSI: 1.2 DME: 3.0 TTE, by mole). Deposition of gel-1 onto the FeF_3 cathodes and electrolyte exchange to yield gel-2, is described in the Experimental Section and the SI.

Figure 1c shows cross-sectional SEM of a representative FeF_3 cathode coated with gel-1. The low vapor pressure for the ILE in gel-1 enabled cross-sectional SEM to be performed without removal of the liquid phase (unlike gel-2, where volatile solvents prevented analogous evaluation). A mixture of FeF_3 and gel-1 is observed above the C-coated Al foil substrate, with an average layer thickness (Figure 1d) of 85 ± 3 μm (N = 201 measurements). Subtracting the average thickness of the uncoated FeF_3 layer (20 ± 5 μm; Figure 1b) from this value, we estimate that gel-1 is ~65 μm thick. This assertion is supported by Figure 1e and 1f, which show that the average gel thickness in the absence of FeF_3 is 62 ± 4 μm (N = 200).

Additional PVDF-HFP gel characterization was accomplished using electrochemical impedance spectroscopy (EIS) and Raman spectroscopy. EIS, in particular, was used to analyze the impact of gel-1 and gel-2 on ionic conductivity (σ), activation energy (E_a), and the charge transfer resistance (R_{CT}) of assembled Li-FeF_3 full cells.

Table 1 shows σ values for each gel as a function of temperature. The value of σ for gel-1 ($\sigma_{Gel\text{-}1}$) at room temperature (0.33 mS cm^{-1}) is ~5-6× times lower than that expected for the unencapsulated ILE (~1.5 mS cm^{-1})[26] and neat $PYR_{14}TFSI$ (~2.0 mS cm^{-1}).[26, 27] By contrast, σ of gel-2 ($\sigma_{Gel\text{-}2}$) at room temperature (1.92 mS cm^{-1}) is close to that previously reported for the unencapsulated LHCE (1.6-2.4 mS cm^{-1}).[28, 29]

There are several important takeaways from Table 1. First, $\sigma_{Gel\text{-}2}$ at room temperature is substantially higher than $\sigma_{Gel\text{-}1}$ at all temperatures (ranging from ~9x higher at 0°C to ~2x higher at 80°C). The fact that $\sigma_{Gel\text{-}2}$ is ~6× higher at 25°C than $\sigma_{Gel\text{-}1}$ makes gel-2 a more promising candidate than gel-1 for use in room temperature pseudo-solid state Li-FeF_3

batteries. Second, $\sigma_{Gel\text{-}2}$ is up to 5 orders of magnitude higher than most polyethylene oxide (PEO)-based separators (typically 10^{-1} to 10^{-5} mS cm^{-1}).[30] Third, to the best of our knowledge, $\sigma_{Gel\text{-}1}$ (0.33 and 1.18 mS cm^{-1} at 25 and 60°C, respectively) and $\sigma_{Gel\text{-}2}$ (1.92 and 3.74 mS cm^{-1} at 25 and 60°C, respectively) are up to one to two orders of magnitude greater than the separators used in previous reports of solid state Li-FeF_3 batteries (highs of 0.03 and 0.31 mS cm^{-1} at 30 and 60°C, respectively).[20-22]

The Arrhenius plots in Figure 2a show that electrolyte exchange with LHCE decreases E_a by ~2×. We hypothesize that higher σ and lower E_a for gel-2, relative to gel-1, is due to the substantially lower viscosity of the LHCE (3.7-4.8 cP)[28, 29] relative to the IL ($PYR_{14}TFSI$; 95.1 cP).[27]

Figure 2b compares representative EIS spectra for Li-FeF_3 full cells containing PVDF-HFP gels (gel-1 and gel-2) with those containing traditional glass fiber type C (GF/C) separators soaked in electrolyte (ILE and LHCE controls). The semicircle at high frequencies represents the charge transfer resistance (R_{CT}). The average R_{CT} values of Li-FeF_3 full cells are 68 ± 28, 128 ± 65, 32 ± 12, and 27 ± 17 Ω for the ILE control (black trace), gel-1 (red trace), gel-2 (blue trace), and the LHCE control (green trace), respectively (N = 3 trials in each case). Although R_{CT} for gel-1 is within experimental error of the ILE control, we note that the average value of the former (128 Ω) is approximately double that of the latter (68 Ω).

After electrolyte exchange of gel-1 with LHCE to yield gel-2, the average R_{CT} decreases by a factor of ~4×. The dramatic decrease in R_{CT} to a value (32 ± 12 Ω) close to that of the LHCE control (27 ± 17 Ω) helps confirm successful electrolyte exchange (further analyzed in the next section). Overall, close values of R_{CT} and σ for gel-2 and the LHCE control highlight the ability of the former to serve as a feasible alternative to a traditional separator in Li-FeF_3 batteries.

Table 1. Ionic conductivity (σ) of the PVDF-HFP gels before and after electrolyte exchange.

Temperature (°C)	σ_{Gel-1}[a] (mS cm^{-1})	σ_{Gel-2}[b] (mS cm^{-1})
0	0.11	0.99
25	0.33	1.92
40	0.67	2.67
60	1.18	3.74
80	2.85	4.94

[a] Ionic conductivity before electrolyte exchange. Gel-1 represents PVDF-HFP filled with ionic liquid electrolyte (ILE = 1.0 M LiFSI in $PYR_{14}TFSI$).

[b] Ionic conductivity after electrolyte exchange with localized high concentration electrolyte (LHCE = 1.0 LiFSI:1.2 DME: 3.0 TTE, by mole) to yield gel-2.

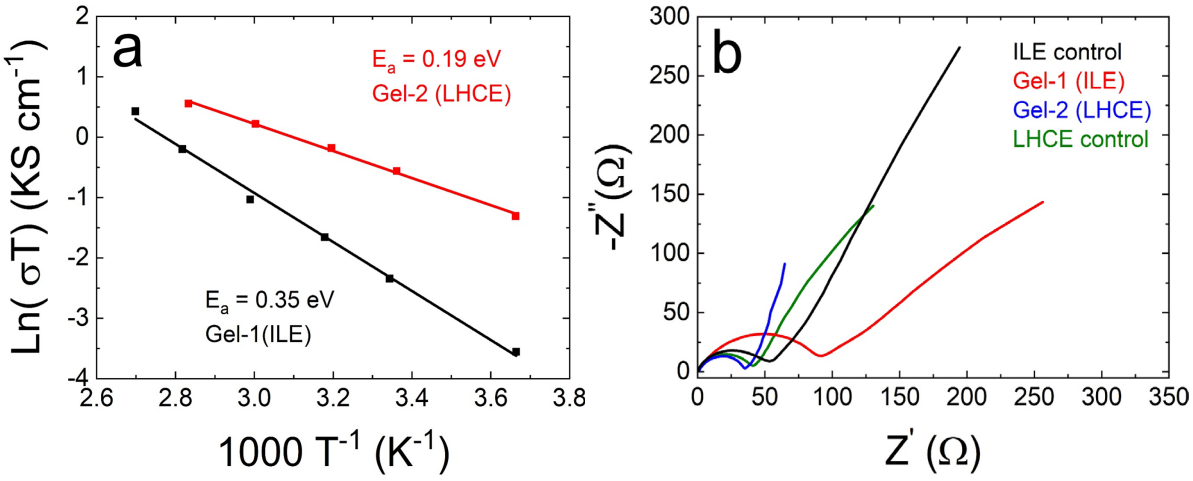

Figure 2. (a) Arrhenius plots for PVDF-HFP gels filled with the electrolytes listed in parentheses (ILE = 1.0 M LiFSI in $PYR_{14}TFSI$ and LHCE = 1.0 LiFSI: 1.2 DME: 3.0 TTE, by mole); calculated activation energies (E_a = -1000 $*$ m $*$ k_B, where m is the slope and k_B is the Boltzmann constant = 8.63x10^{-5} eV K^{-1}) are indicated in the plot. (b) Representative Nyquist plots for Li-FeF_3 full cells using either gel separators or traditional (glass fiber) separators (ILE and LHCE controls).

Raman spectroscopy. Figure S2a shows the complete Raman spectra of the PVDF-HFP gels before (gel-1) and after (gel-2) electrolyte exchange, with accompanying comparison to their pure components (ILE, LHCE, and PVDF-HFP). The Raman spectrum of the pure ILE standard (Figure S2a, black trace) is nearly identical to that of gel-1 (red trace), with the exception of several peaks originating from PVDF-HFP (Figure S2b and S2c). Likewise, the spectrum for gel-2 (Figure S2a, green trace) is similar to that of pure LHCE (purple trace). The contribution of PVDF-HFP (blue trace) to gel-2 is discussed later.

Two sets of changes in Figure 3 confirm successful replacement of the ILE in gel-1 with LHCE in gel-2. First, the characteristic peaks of the IL anion ($TFSI^-$; 277, 296, 311, 339, 371, and 400 cm^{-1})[31, 32] observed in Figure 3a for the pure ILE (black trace) and gel-1 (red trace) disappear for gel-2 (green trace). Indeed, only peaks due to FSI^- (292, 327, 357, 458, and 488 cm^{-1}) [33, 34] remain in this spectral region (~200-500 cm^{-1}) for gel-2. This scenario is as expected upon electrolyte exchange, given the lack of $TFSI^-$ anions in the LHCE (purple trace; 1.0 LiFSI:1.2 DME:3.0 TTE, by mole). We note that the higher intensity of the FSI^- peaks in the LHCE-containing samples reflects the higher concentration of FSI^- (1.7 M LiFSI) relative to the ILE (1.0 M LiFSI).

Second, the characteristic peaks [31, 35, 36] of the IL cation (PYR_{14}^+) observed in Figure 3b (799, 823, 880, 902, 925, 1000, 1030, 1057) and 3c (2882, 2949, 2974, 2998, and 3031-3046 cm^{-1}) for the pure ILE (black traces) and gel-1 (red traces) are absent in gel-2 (green traces). The only peaks in gel-2 that roughly match those expected for PYR_{14}^+ (797, 811, 838, 877, 2978, and 3014 cm^{-1}) are better explained by the presence of PVDF-HFP (793-796, 870-872, 879-881, and 2981-2985 cm^{-1}),[37-39] the rise of polar (β and γ) PVDF phases (Figure S3; 811, 838, 881, and 3016-3017 cm^{-1}), [37-39] and Li-DME coordination (879 cm^{-1}).[40]

Overall, Figure 3a-c shows that the peaks due to both the IL anion and cation disappear in the Raman spectra for gel-2. Furthermore, the Raman spectra for gel-2 and the

pure LHCE bear close resemblance. Together, these results lead us to conclude that the electrolyte exchange is successful and complete.

The presence of the β PVDF phase in gel-2 (Figure S3) is noteworthy. Segregation of -CF_2 and -CH_2 groups on opposite sides of the polymer in that phase facilitates cation hopping, which can improve cation mobility.[41, 42] Although the β PVDF phase can be difficult to obtain, its formation can be fast tracked by simply incorporating an ILE into PVDF[43] or PVDF-HFP.[41] The ILs used in those cases[41, 43] (e.g., [BMIM][PF_6] and EMIMTFSI) have relative dielectric constants (12-16)[44, 45] similar to the IL in gel-1 (ε (PYR_{14}TFSI) = 14.7).[44] The fact that gel-1 was used as a template for gel-2 could help explain the appearance of the β phase in gel-2. Alternative explanations are discussed in the SI.

In addition to confirming electrolyte exchange, the Raman spectra in Figure 3d provide insights into the LHCE solvent structure and electrolyte-polymer interactions. These topics are discussed in detail in the SI (Figure S4, Table S1, and Figure S5). Briefly, the high extent of Li^+FSI^- coordination (~99-100%) in the pure LHCE and gel-2 confirms that the HCE property of the LHCE is intact in each case. Shifts in the type of Li^+FSI^- ion pairs, on the other hand, suggest the possibility of electrolyte-polymer interactions.

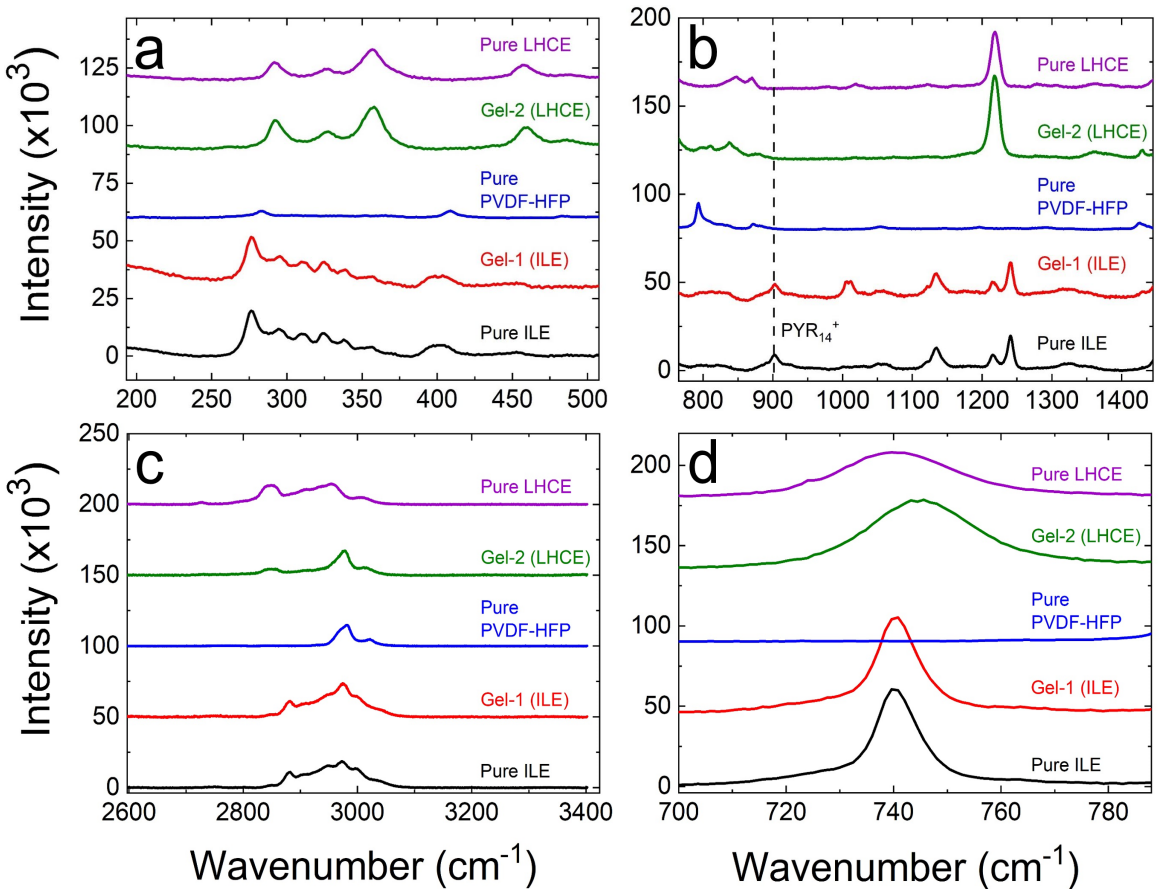

Figure 3. Raman spectra of the gels and their components (PVDF-HFP, ILE = 1.0 M LiFSI in $PYR_{14}TFSI$, and LHCE = 1.0 LiFSI: 1.2 DME: 3.0 TTE, by mole), in regions characteristic for: (a) $TFSI^-/FSI^-$, (b,c) PYR_{14}^+, and (d) $Li^+FSI^-/TFSI^-$ coordination. The range in (b) extends past that of PYR_{14}^+ (~800-1100 cm^{-1}) to sharpen relevant peaks (dashed line = main PYR_{14}^+ peak in that region).

Stability of the PVDF-HFP gels with the anode and cathode. As discussed in the Introduction, instabilities with both FeF_3[1, 7] and Li metal[3, 16, 22] contribute to low coulombic efficiency (CE) in Li-FeF_3 batteries. Following our recent demonstration that the LHCE is stable with both the Li metal anode and FeF_3 cathode,[19] we used Li half-cells and FeF_3 half cells to evaluate stability of these electrodes with gel-2.

Li half-cells were prepared as described in the Experimental Section and SI. Briefly, each cell contained a Li anode and a current collector (either a stainless steel (SS) spacer or

Cu foil), separated by either gel-2 or by a traditional (Celgard) separator soaked in electrolyte (LHCE control). Figure 4a compares the Li half-cell CE over 50 cycles for the former (black trace) and latter (red and blue traces) cases, at a current density of 1.0 mA cm^{-2} (= 1 C) and a capacity of 1.0 mAh cm^{-2}. We note that an SS current collector was chosen for gel-2, rather than Cu foil (the conventional choice[46] for Li half-cells), because it provided a flatter surface for gel deposition. Comparison of the average Li half-cell CE over 50 cycles for the red (98.3 ± 0.9%) and blue (98.5 ± 0.6%) traces indicates that no significant artifacts are introduced by this choice.

Overall, the average Li CE over 50 cycles for gel-2 coated SS (98 ± 2%) is statistically indistinguishable from that of the LHCE control using SS (98.3 ± 0.9%). This result bolsters the assertion made earlier that gel-2 is a promising alternative for a traditional separator in Li-FeF_3 batteries.

FeF_3 half-cells were constructed by pairing FeF_3 cathodes (with or without gel-2) with partially delithiated LFP ($Li_{0.66}FePO_4$). Partially delithiated LFP was chosen as a counter electrode in these cells due to its highly stable reference potential (~3.4 V vs. Li/Li^+),[47-49] which is similar to the open circuit potentials that we observed for the Li-FeF_3 full cells (~3.3-3.5 V vs. Li/Li^+).

The partially delithiated LFP (Figure S6a) and the corresponding FeF_3 half-cells (Figure S6b-d, S7, and S8) are characterized in the SI. There are two important conclusions from that analysis. First, the electrochemical characteristics of the FeF_3 half-cells correspond closely with those of the Li-FeF_3 full cells. More specifically, similar galvanostatic (GV) profiles (Figure S6b, S6c, S9a, and S9b) and capacities (Figure S7 and S8) are obtained. These similarities suggest that the FeF_3 half-cells are adequately representative of the Li-FeF_3 full cells to enable comparison. Second, cyclic voltammetry (Figure S6d) indicates that the FeF_3 cathodes are chemically stable with respect to gel-2.

By analogy to the Li half-cells, the stability of gel-2 with FeF_3 was assessed by evaluating the average FeF_3 half-cell CE over 50 cycles at 1.0 mA cm^{-2} (Figure 4b). The average FeF_3 half-cell CE using these conditions is 95 ± 6% for gel-2 (black trace) and 94 ± 6% for the LHCE control (red trace). These values are remarkably similar to those obtained using the same conditions for Li-FeF_3 full cells (Figure 4c; 95 ± 5% and 96 ± 4% for gel-2 and the LHCE control, respectively).

Interestingly, the Li half-cell CE for gel-2 at 1.0 mA cm^{-2} starts higher (average of 95.0% on the first cycle) than either the FeF_3 half-cell (53.0%) or Li-FeF_3 full cell (59.8%) CEs. Although CEs for the Li half-cells, FeF_3 half-cells, and Li-FeF_3 full cells stabilize after a similar number of cycles (~4-7), the Li half-cells achieve consistent CE values ≥97% more rapidly (by ~4-6 cycles) than the latter two cells (~33-45 and ~25-30 cycles, respectively). Overall, these results suggest that the solid electrolyte interface (SEI) is established more rapidly than the cathode electrolyte interface (CEI). In both the half-cells and full cells, high CEs are ultimately obtained. The average 50^{th} cycle CE at 1.0 mA cm^{-2} using gel-2 is 99.2 , 97.1, and 98.0 % for the Li half-cells, FeF_3 half-cells, and Li-FeF_3 full cells, respectively.

Gradual CEI formation is consistent with our previous report of Li-FeF_3 full cells cycled with unencapsulated LHCE,[19] where ~20-30 cycles were required to stabilize capacity fade at a rate of C/20 (equivalent to 0.05 mA cm^{-2} in the present report). Although we cannot completely rule out the influence of current density on the rate of CEI stabilization, Figure S10 suggests that this process is more dependent on the number of initial cycles than on the particular current density.

Figure S11 shows that when 20 prior cycles are performed at slower rates, the average CE at 1.0 mA cm^{-2} for the gel-2 and LHCE control FeF_3 half-cells (over 50 subsequent cycles) increases to 98 ± 3% and 99 ± 3%, respectively. These CEs are similar to those obtained for the Li-FeF_3 full cells cycled with identical conditions (Figure 4d; 99 ± 3% and 98 ± 4%, respectively). Figure S11 and Figure 4d collectively demonstrate that although CEI

buildup lags behind SEI buildup, ≥98% CE is ultimately obtained. High CE with both the Li half-cells and FeF_3 half-cells suggests that gel-2 is stable with both the Li metal anode and the FeF_3 cathode.

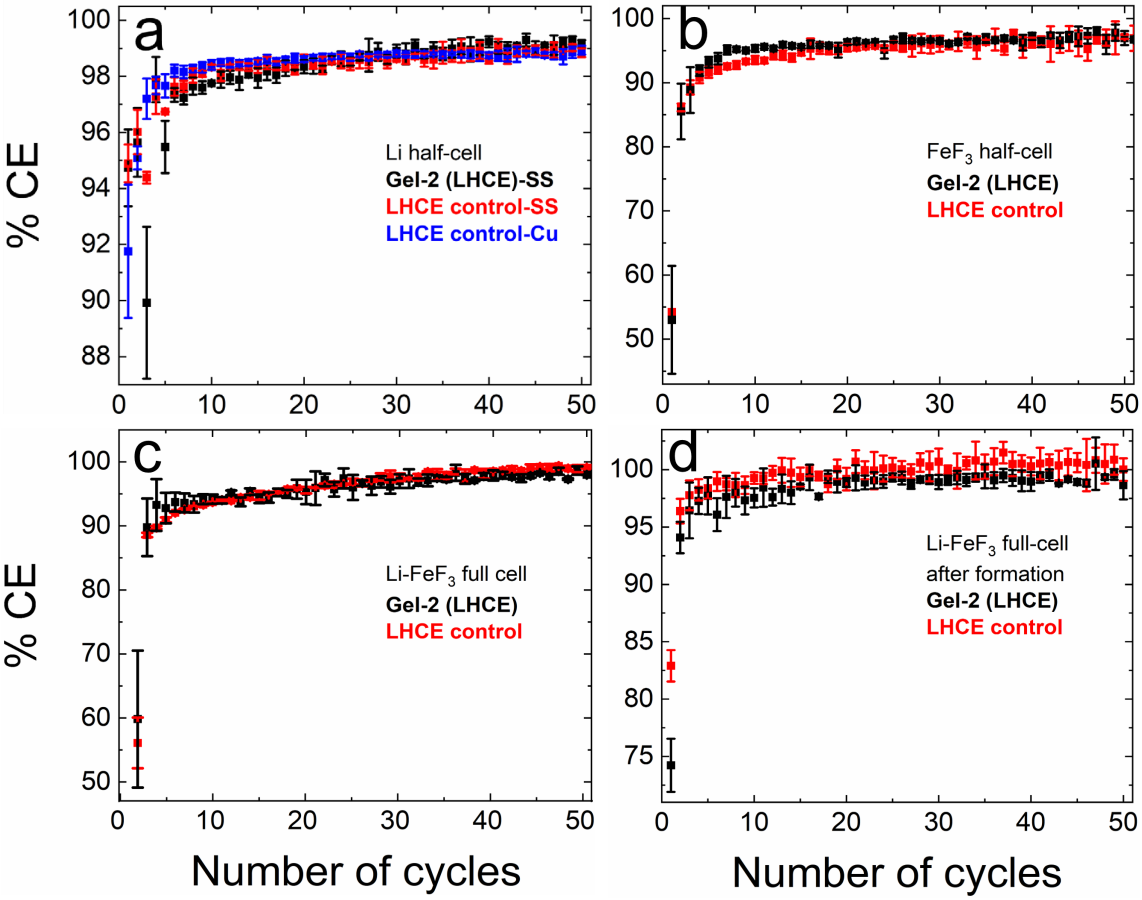

Figure 4. Percent coulombic efficiency (% CE) at 1.0 mA cm^{-2} (= 1 C) for (a) Li half-cells (with either SS = stainless steel or Cu current collectors), (b) FeF_3 half-cells, and (c,d) Li-FeF_3 full cells, assembled using either gel-2 (PVDF-HFP filled with LHCE = 1.0 LiFSI: 1.2 DME: 3.0 TTE, by mole) or traditional separators (LHCE control; (a) Celgard, (b,d) glass fiber). CEs in (d) were assessed after 20 formation cycles at slower rates (e.g., the rate testing protocol in Figure 5a).

Electrochemical rate testing. Figure 5a compares Li-FeF_3 rate testing for gel-1, gel-2, and an LHCE control (no gel) at current densities ranging from 0.05-0.50 mA cm^{-2} (= C/20

to C/2; five cycles each). Before discussing the main results, it is worth pointing out several features in the initial five cycles at 0.05 mA cm^{-2}. Briefly, the slightly greater than theoretical (712 mAh g^{-1}) initial discharge capacities and steep capacity drop between the first and second cycles (~14-19%) are believed to be due to CEI formation in iron fluoride batteries.[19, 20] Furthermore, the downward sloping trend in the initial five cycles is consistent with our previous finding that Li-FeF_3 capacity fade requires ~20-30 cycles at C/20 (or 0.05 mA cm^{-2} in the present report) to stabilize in LHCE.[19] Figure 5 shows that cycle stability improves at higher current densities (0.10 to 1.0 mA cm^{-2} = C/10 to 1 C). As discussed in the previous section, Figure S10 suggests that the number of initial cycles (rather than the particular current density) governs capacity fade stabilization. We note, however, that kinetic limitations could also play a role in stabilizing capacity fade at faster rates. For example, more reversible steps (e.g., the insertion step to form $Li_xFe_yF_3$) could be favored over kinetically sluggish steps (e.g., the conversion reaction)[1] at faster rates. Indeed, Figure S9c and Table S2 show that preference for the conversion reaction decreases by a small but significant (~7%) amount from 0.05 to 1.0 mA cm^{-2}.

Overall, there are three important takeaways from Figure 5. First, the cycling performance obtained with gel-2 across a range of current densities (0.05-0.50 mA cm^{-2}) matches that of the LHCE control. We reiterate that gel-2 has the added advantage of flexibility, which helps the cell adapt to the large volume changes expected during iron fluoride conversion reactions (up to 30%).[20]

Despite similar Li-FeF_3 full cell performance at 0.05-0.50 mA cm^{-2} for gel-2 and the LHCE control, the capacities of the former are approximately half that of the latter at the fastest rate tested (1.0 mA cm^{-2} = 1 C; Figure 5b). We hypothesize that the gap in cycling performance at 1.0 mA cm^{-2} between gel-2 and the LHCE control is due to slower ion transport in the presence of the gel. For example, polymer gels have a tendency to be non-Newtonian and thus dependent on shear rate.[50] Non-uniformity in gel thickness (e.g., as a

result of the dropcasting procedure used here) can decrease Li^+ ion mobility.[51] Although this discrepancy might be small enough to go undetected for gel-2 at slow rates (due to the low viscosity of the LHCE), it may become significant at faster rates (where ohmic losses and the demands of ion transport are greater).

Second, electrolyte exchange of gel-1 to yield gel-2 results in superior cycling performance. Although the capacities for these two gels are comparable at 0.05 mA cm^{-2}, they become progressively disparate at higher current densities (0.10 to 1.0 mA cm^{-2}). More specifically, the capacities for gel-2 surpass those of gel-1 by factors of 1.7×, 3.2×, 4.7×, and 4.5× at 0.10, 0.20, 0.50, and 1.0 mA cm^{-2}, respectively. As discussed in Figure S13, ionic conductivity differences alone are an inadequate explanation for this trend. Instead, we attribute these results to three factors: viscosity (~20-26× lower for the LHCE;[27-29] *vide supra*), R_{CT} (~4x lower for gel-2 than gel-1; Figure 2b), and the unique solvent structure of LHCEs. Lower viscosity for the LHCE in gel-2 allows for greater Li^+ ion mobility, which is increasingly important at faster rates. Greater R_{CT} for gel-1 results in more polarization than gel-2 at high current densities (Figure S14), which translates to lower capacities.

Better resistance to side reactions with gel-2 is most clearly demonstrated by the Li-FeF_3 full cell CE values at 1.0 mA cm^{-2} (Figure S12). In particular, the average Li-FeF_3 full cell CE for gel-1 (101 ± 3% across 50 cycles) exceeds 100%. The average full cell CE for gel-2 at 1.0 mA cm^{-2}, on the other hand, is 98 ± 4%. These trends reflect the fact that the LHCE is less prone to side reactions than the ILE.

Third, in the present report we obtain room temperature Li-FeF_3 capacities at 0.05-0.50 mA cm^{-2} with gel-2 (Figure 5 and Table S3) that, to the best of our knowledge, were previously only accessible at elevated temperatures (50-60°C)[20-22] for solid state Li-FeF_3 batteries (Table S4). This point is most clearly demonstrated by comparison of our results to prior work in terms of current density (Table S5) rather than C-rate (particularly for 1.0 mA cm^{-2}) to account for the fact that our mass loading was ~2× higher.

As a final point, we briefly discuss preliminary results at 60°C. Figure S15 shows that elevated temperature confers only moderate benefit for gel-2. Performance for gel-1, on the other hand, improves dramatically. Indeed, gel-1 becomes a viable contender to gel-2 at elevated temperature. This topic is further discussed in the SI. Briefly, the boosted capacities for gel-1 are likely due to decreased viscosity of the ILE at 60°C, along with faster kinetics and increased gel flexibility. We note that improved performance for gel-1 at 60°C is limited to lower current densities. Beyond 0.50 mA cm^{-2}, the capacities decay to their room temperature values. Additional experiments are needed for further elucidation.

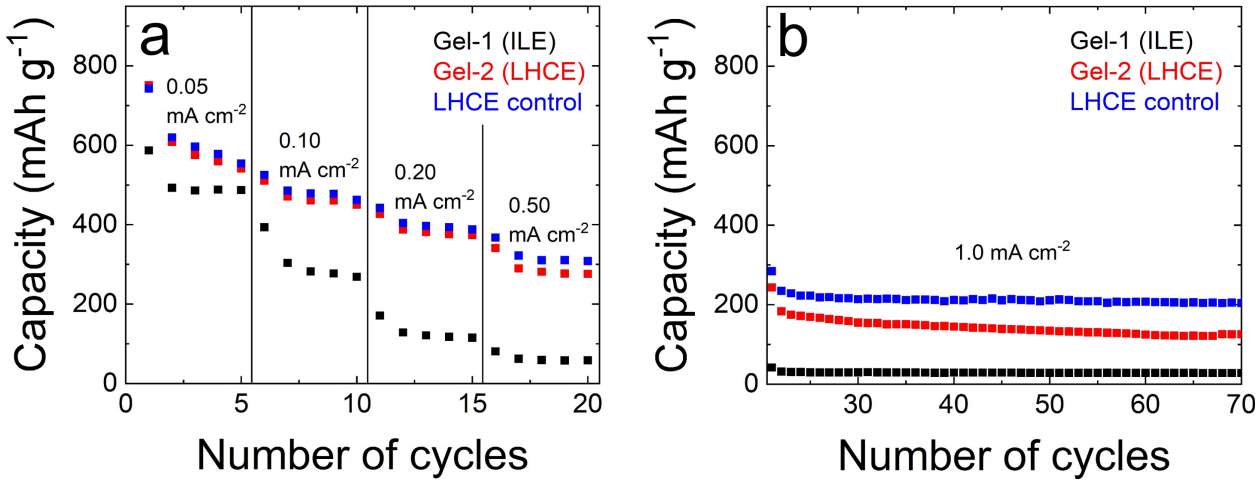

Figure 5. Electrochemical rate testing at (a) 0.05-0.50 mA cm^{-2} (= C/20 to C/2) and (b) 1.0 mA cm^{-2} (= 1 C) for Li-FeF_3 full cells containing a 1.3 cm^2 bulk Li anode, 1.6 cm^2 FeF_3 cathode (1.4-1.9 mg cm^{-2}), and either a PVDF-HFP gel separator filled with one of the electrolytes listed in parentheses (ILE = 1.0 M LiFSI in $PYR_{14}TFSI$ and LHCE = 1.0 LiFSI: 1.2 DME: 3.0 TTE, by mole) or a traditional glass fiber separator soaked in electrolyte (LHCE control).

Conclusions

In this report, we have demonstrated the fabrication and detailed characterization of room temperature pseudo-solid state batteries containing Li anodes and FeF_3 conversion cathodes that operate at high current density (1.0 mA cm^{-2}). The improvement over prior work, which required elevated temperatures to achieve similar performance,[20-22] is enabled by our use of a conformal PVDF-HFP gel filled with a localized high concentration electrolyte (LHCE). We attribute this improvement to the ionic conductivity of the LHCE-filled gel (1.92 mS cm^{-1} at 25°C), which exceeds that of the latter[20-22] by up to two orders of magnitude. In addition to room temperature operation, the LHCE gel prevents side reactions and is stable with both the Li anode and FeF_3 cathode, as evidenced by coulombic efficiencies >98% for Li-FeF_3 full cells, Li half-cells, and FeF_3 half-cells.

The particular LHCE evaluated in the present report was tailored to the Li-FeF_3 system. However, the concept of using an LHCE-filled PVDF-HFP gel (regardless of the type of LHCE) to simultaneously mitigate side reactions and provide the flexibility needed to adapt to conversion-reaction related volume changes has the potential to be broadly applicable.

Finally, although we primarily evaluated cycling performance at a single temperature (25°C), the relatively high ionic conductivity (~1-5 mS cm^{-1}) of the LHCE gel from 0-80°C expands the scope of our findings to systems requiring lower and higher temperatures (e.g., electric vehicles in cold weather). Preliminary experiments at 60°C show promise for an alternative PVDF-HFP gel filled with an ionic liquid electrolyte (1.0 M LiFSI in $PYR_{14}TFSI$). The ILE-filled gel represents a safer alternative to the LHCE-filled gel due to the negligible vapor pressure of the ILE.[12]

Experimental Section

Coin cell preparation. A complete description of the materials and experimental procedures used to prepare electrodes, PVDF-HFP gels, and the associated coin cells is provided in the SI. Briefly, cathodes were obtained by dropcasting a slurry containing 70% FeF_3, 20% Super

P, and 10% PVDF binder onto C-coated Al foil disks. After baking to remove residual water, the FeF_3 cathodes were coated with gel-1, which consisted of PVDF-HFP filled with an ionic liquid electrolyte (ILE = 1.0 M LiFSI in $PYR_{14}TFSI$). Gel-1 coated cathodes were either used as prepared or exchanged with a localized high concentration electrolyte (LHCE = 1.0 LiFSI: 1.2 DME: 3.0 TTE, by mole) to yield gel-2. Li-FeF_3 coin cells used a 1.6 cm^2 gel-coated FeF_3 cathode (1.4-1.9 mg cm^{-2}), 1.3 cm^2 bulk Li anode (0.6 mm thick), 0.7 mm of stainless steel spacers (0.5 mm below the anode and 0.2 mm above the cathode), a Belleville washer spring, and CR2032 coin cases. A small GF/C ring (1.98 cm^2 with a 0.87 cm^2 hole in the center) was used to protect just the edges of each cathode, where gel coating could be spotty. Each coin cell was crimped at a pressure of 0.75 ton. For the ILE and LHCE control coin cells, a traditional separator (1.98 cm^2 GF/C) soaked in electrolyte (100 µL of ILE or LHCE) was used in place of the gels.

Li half-cells (FeF_3-free) contained a 2.01 cm^2 Li anode (50 µm on 10 µm Cu foil) sandwiched together with a gel-coated current collector (either stainless steel or Cu foil). FeF_3 half-cells (Li-free) contained a 1.6 cm^2 partially delithiated LFP counter electrode (6.8-7.1 mg cm^{-2}) and a 0.32 cm^2 gel-coated FeF_3 cathode (1.3-1.6 mg cm^{-2}).

Electrochemical cycling. Details regarding characterization of the electrodes and gels are provided in the SI. Briefly, FeF_3 cathodes were characterized via scanning electron microscopy (SEM), Raman spectroscopy, and x-ray diffraction (XRD). Gels were characterized using cross-sectional SEM, Raman spectroscopy, and electrochemical impedance spectroscopy (EIS). Galvanostatic (GV) rate testing of the Li-FeF_3 full cells was performed between 1.0-4.0 V (vs. Li/Li^+) at 0.05-1.0 mA cm^{-2} (equivalent to ~C/20 to 1 C). Five cycles (each) were recorded at 0.05-0.50 mA cm^{-2}, followed by 50 cycles at 1.0 mA cm^{-2}. For the Li half-cells, a predetermined capacity of Li (1.0 mAh cm^{-2}) was electrodeposited and then electrodissolved (at the same specified current) up until a voltage cutoff of 1.0 V vs. Li/Li^+. The cycling procedure for the FeF_3 half-cells was similar to that of the Li-FeF_3 full

cells except the voltage range was 0.6 to -2.4 V (vs. LFP). Potentials for the FeF_3 half-cell experiments were converted to the Li/Li^+ potential scale using the formula $E_{Li/Li^+} = E_{LFP} + 3.43$ V, in accordance with the literature.[47-49] Coulombic efficiency (CE) was determined at 1.0 mA cm^{-2}, over 50 cycles, for both half-cell and full-cell experiments.

Supporting Information

The Supporting Information (SI) is available free of charge on the ACS publications webpage at DOI: https://pubs.acs.org/doi/xx. Detailed experimental procedures; characterization of the ball-milled FeF_3/C powder; complete Raman spectra of the PVDF-HFP gels; evidence of the rise of polar PVDF phases; discussion of localized high concentration electrolyte (LHCE) structure and polymer interactions; electrochemical characterization of cells containing partially delithiated LFP; comparison of rate testing for Li-FeF_3 full cells and FeF_3 half-cells with and without a PVDF-HFP gel separator; discharge/charge profiles of the Li-FeF_3 full cells; fractional contribution of the Li-FeF_3 conversion reaction to the overall discharge capacities; the dependence of Li-FeF_3 cycle stability on cycle number; percent coulombic efficiency (% CE) at various rates for representative FeF_3 half-cells; comparison of the Li-FeF_3 full cell CEs for each PVDF-HFP gel; rate testing for a representative Li-FeF_3 full cell using a traditional separator soaked in ionic liquid electrolyte; the extent of electrochemical polarization at 1.0 mA cm^{-2} for each PVDF-HFP gel; comparison of Li-FeF_3 full cell discharge capacities to previous solid state Li-FeF_3 batteries; galvanostatic cycling at elevated temperature (DOC).

Acknowledgments

This paper describes objective technical results and analysis. Any subjective views or opinions that might be expressed in the paper do not necessarily represent the views of the U.S. Department of Energy or the United States Government. This work was supported by the

Laboratory Directed Research and Development program at Sandia National Laboratories, a multi-mission laboratory managed and operated by National Technology and Engineering Solutions of Sandia, LLC., a wholly owned subsidiary of Honeywell International, Inc., for the U.S. Department of Energy's National Nuclear Security Administration under contract DE-NA-0003525.

Conflict of Interest

The authors declare no competing financial interest.

References

1. Fan, X.; Hu, E.; Ji, X.; Zhu, Y.; Han, F.; Hwang, S.; Liu, J.; Bak, S.; Ma, Z.; Gao, T.; Liou, S.-C.; Bai, J.; Yang, X.-Q.; Mo, Y.; Xu, K.; Su, D.; Wang, C., High energy-density and reversibility of iron fluoride cathode enabled via an intercalation-extrusion reaction. *Nat. Commun.* **2018,** *9*, 2324.

2. Wu, F.; Yushin, G., Conversion cathodes for rechargeable lithium and lithium-ion batteries. *Energy Environ. Sci.* **2017,** *10*, 435-459.

3. Cheng, X.-B.; Zhang, R.; Zhao, C.-Z.; Zhang, Q., Towards Safe Lithium Metal Anode in Rechargeable Batteries: A Review. *Chem. Rev.* **2017,** *117*, 10403-10473.

4. Cho, S.-J.; Yu, D.-E.; Pollard, T. P.; Moon, H.; Jang, M.; Borodin, O.; Lee, S.-Y., Nonflammable Lithium Metal Full Cells with Ultra-high Energy Density Based on Coordinated Carbonate Electrolytes. *iScience* **2020,** *23*, 100844.

5. Fu, W.; Zhao, E.; Sun, Z.; Ren, X.; Magasinski, A.; Yushin, G., Iron Fluoride-Carbon Nanocomposite Nanofibers as Free-Standing Cathodes for High-Energy Lithium Batteries. *Adv. Funct. Mater.* **2018,** *28*, 1801711.

6. Shen, Y.; Wang, X.; Hu, H.; Jiang, M.; Yang, X.; Shu, H., A graphene loading heterogeneous hydrated forms iron based fluoride nanocomposite as novel and high-capacity cathode material for lithium/sodium ion batteries. *J. Power Sources* **2015,** *283*, 204-210.

7. Wu, F.; Srot, V.; Chen, S.; Lorger, S.; van Aken, P. A.; Maier, J.; Yu, Y., 3D Honeycomb Architecture Enables a High-Rate and Long-Life Iron (III) Fluoride-Lithium Battery. *Adv. Mater.* **2019,** *31*, 1905146.

8. Ren, X.; Chen, S.; Lee, H.; Mei, D.; Engelhard, M.H.; Burton, S. D.; Zhao, W.; Zheng, J.; Li, Q.; Ding, M. S.; Schroeder, M.; Alvarado, J.; Xu, K.; Meng, Y.S.; Liu, J.; Zhang, J.-G.; Xu, W., Localized High-Concentration Sulfone Electrolytes for High-Efficiency Lithium-Metal Batteries. *Chem* **2018,** *4*, 1877-1892.

9. Xia, S.; Wu, X.; Zhang, Z.; Cui, Y.; Liu, W., Practical Challenges and Future Perspectives of All-Solid-State Lithium-Metal Batteries. *Chem* **2019,** *5*, 753-785.

10. Liu, J.; Bao, Z.; Cui, Y.; Dufek, E. J.; Goodenough, J. B.; Khalifah, P.; Li, Q.; Yann Liaw, B.; Liu, P.; Manthiram, A.; Meng, Y.S.; Subramanian, V.R.; Toney, M.F.; Viswanathan, V.V.; Whittingham, M.S.; Xiao, J.; Xu, W.; Yang, J.; Yang, X.-Q.; Zhang, J.-G., Pathways for practical high-energy long-cycling lithium metal batteries. *Nat. Energy* **2019,** *4*, 180-186.

11. Ashby, D. S.; DeBlock, R. H.; Lai, C.-H.; Choi, C. S.; Dunn, B. S., Patternable, Solution-Processed Ionogels for Thin-Film Lithium-Ion Electrolytes. *Joule* **2017,** *1*, 344-358.

12. Le Bideau, J.; Viau, L.; Vioux, A., Ionogels, ionic liquid based hybrid materials. *Chem. Soc. Rev.* **2011,** *40*, 907-925.

13. Ashby, D. S.; DeBlock, R. H.; Choi, C. S.; Sugimoto, W.; Dunn, B., Electrochemical and Spectroscopic Analysis of the Ionogel-Electrode Interface. *ACS Appl. Mater. Interfaces* **2019,** *11*, 12088-12097.

14. Ashby, D. S.; Cardenas, J. A.; Bhandarkar, A.; Cook, A.; Talin, A. A., Modifying Ionogel Solid-Electrolytes for Custom Applications. *ACS Appl. Energy Mater.* **2022**, submitted.

15. Zhou, D.; Shanmukaraj, D.; Tkacheva, A.; Armand, M.; Wang, G., Polymer Electrolytes for Lithium-Based Batteries: Advances and Prospects. *Chem* **2019,** *5*, 2326-2352.

16. Chen, S.; Zheng, J.; Mei, D.; Han, K. S.; Engelhard, M. H.; Zhao, W.; Xu, W.; Liu, J.; Zhang, J.-G., High-Voltage Lithium-Metal Batteries Enabled by Localized High-Concentration Electrolytes. *Adv. Mater.* **2018,** *30*, 1706102.

17. Leng, Y.; Ge, S.; Yang, X.-G.; Longchamps, R. S.; Liu, T.; Wang, C.-Y., Fast Charging of Energy-Dense Lithium Metal Batteries in Localized Ether-Based Highly Concentrated Electrolytes. *J. Electrochem. Soc.* **2021,** *168*, 060548.

18. Gu, W.; Borodin, O.; Zdyrko, B.; Lin, H.-T.; Kim, H.; Nitta, N.; Huang, J.; Magasinski, A.; Milicev, Z.; Berdichevsky, G.; Yushin, G., Lithium-Iron Fluoride Battery with In Situ Surface Protection. *Adv. Funct. Mater.* **2016,** *26*, 1507-1516.

19. Wygant, B. R.; Merrill, L. C.; Harrison, K. L.; Talin, A. A.; Ashby, D. S.; Lambert, T. N., The Role of Electrolyte Composition in Enabling Li Metal-Iron Fluoride Full-cell Batteries. *Adv. Sci.* **2022**, 2105803.

20. Huang, Q.; Turcheniuk, K.; Ren, X.; Magasinski, A.; Song, A.-Y.; Xiao, Y.; Kim, D.; Yushin, G., Cycle stability of conversion-type iron fluoride lithium battery cathode at elevated temperatures in polymer electrolyte composites. *Nat. Mater.* **2019,** *18*, 1343-1349.

21. Hu, J.; Chen, K.; Yao, Z.; Li, C., Unlocking solid-state conversion batteries reinforced by hierarchical microsphere stacked polymer electrolyte. *Sci. Bull.* **2021,** *66*, 694-707.

22. Wu, X.; Chen, K.; Yao, Z.; Hu, J.; Huang, M.; Meng, J.; Ma, S.; Wu, T.; Cui, Y.; Li, C., Metal organic framework reinforced polymer electrolyte with high cation transference number to enable dendrite-free solid state Li metal conversion batteries. *J. Power Sources* **2021,** *501*, 229946.

23. La Mantia, F.; Wessells, C. D.; Deshazer, H. D.; Cui, Y., Reliable reference electrodes for lithium-ion batteries. *Electrochem. Commun.* **2013,** *31*, 141-144.

24. Ishige, Y.; Klink, S.; Schuhmann, W., Intercalation Compounds as Inner Reference Electrodes for Reproducible and Robust Solid-Contact Ion-Selective Electrodes. *Angew. Chem. Int. Ed.* **2016,** *55*, 4831-4835.

25. Wandt, J.; Lee, J.; Arrigan, D. W. M.; Silvester, D. S., A lithium iron phosphate reference electrode for ionic liquid electrolytes. *Electrochem. Commun.* **2018,** *93*, 148-151.

26. Shepherd, I. W., Raman scattering in FeF3. *Phys. Lett. A* **1973,** *43*, 305-306.

27. Guerin, K.; Delbegue, D.; Louvain, N.; Doubtsof, L.; Hamwi, A.; Laik, B.; Pereira-Ramos, J.-P.; Tahar-sougrati, M.; Jumas, J.-C.; Willmann, P.; Cenac-Morthe, C.,

Rhombohedral iron trifluoride with a hierarchized macroporous/mesoporous texture from gaseous fluorination of iron disilicide. *Mater. Chem. Phys.* **2016,** *173*, 355-363.

28. Maslova, O. A.; Ammar, M. R.; Guimbretiere, G.; Rouzaud, J.-N.; Simon, P., Determination of crystallite size in polished graphitized carbon by Raman spectroscopy. *Phys. Rev. B* **2012,** *86*, 134205.

29. Nadherna, M.; Reiter, J.; Moskon, J.; Dominko, R., Lithium bis(fluorosulfonyl)imide-PYR_{14}TFSI ionic liquid electrolyte compatible with graphite. *J. Power Sources* **2011,** *196*, 7700-7706.

30. Johansson, P.; Fast, L. E.; Matic, A.; Appetecchi, G. B.; Passerini, S., The conductivity of pyrrolidinium and sulfonylimide-based ionic liquids: A combined experimental and computational study. *J. Power Sources* **2010,** *195*, 2074-2076.

31. Ren, X.; Gao, P.; Zou, L.; Xu, W., Role of inner solvation sheath within salt-solvent complexes in tailoring electrode/electrolyte interphases for lithium metal batteries. *Proc. Natl. Acad. Sci. USA* **2020,** *117*, 28603-28613.

32. Ren, X.; Zou, L.; Cao, X.; Engelhard, M. H.; Liu, W.; Burton, S. D.; Lee, H.; Niu, C.; Matthews, B. E.; Zhu, Z.; Wang, C.; Arey, B.W.; Xiao, J.; Liu, J.; Zhang, J.-G.; Xu, W., Enabling High-Voltage Lithium-Metal Batteries under Practical Conditions. *Joule* **2019,** *3*, 1662-1676.

33. Xue, Z.; He, D.; Xie, X., Poly(ethylene oxide)-based electrolytes for lithium-ion batteries. *J. Mater. Chem. A* **2015,** *3*, 19218-19253.

34. Capitani, F.; Trequattrini, F.; Palumbo, O.; Paolone, A.; Postorino, P., Phase Transitions of PYR_{14}-TFSI as a Function of Pressure and Temperature: the Competition between Smaller Volume and Lower Energy Conformer. *J. Phys. Chem. B* **2016,** *120*, 2921-2928.

35. Umebayashi, Y.; Mitsugi, T.; Fukuda, S.; Fujimori, T.; Fujii, K.; Kanzaki, R.; Takeuchi, M.; Ishiguro, S.-I., Lithium Ion Solvation in Room-Temperature Ionic Liquids

Involving Bis(trifluoromethanesulfonyl) Imide Anion Studied by Raman Spectroscopy and DFT Calculations. *J. Phys. Chem. B* **2007,** *111*, 13028-13032.

36. Liu, X.; Zarrabeitia, M.; Mariani, A.; Gao, X.; Schutz, H. M.; Fang, S.; Bizien, T.; Elia, G. A.; Passerini, S., Enhanced Li^+ Transport in Ionic Liquid-Based Electrolytes Aided by Fluorinated Ethers for Highly Efficient Lithium Metal Batteries with Improved Rate Capability. *Small Methods* **2021,** *5*, 2100168.

37. Fujii, K.; Seki, S.; Fukuda, S.; Kanzaki, R.; Takamuku, T.; Umebayashi, Y.; Ishiguro, S.-I., Anion Conformation of Low-Viscosity Room-Temperature Ionic Liquid 1-Ethyl-3-methylimidazolium Bis(fluorosulfonyl) Imide. *J. Phys. Chem. B* **2007,** *111*, 12829-12833.

38. Kunze, M.; Jeong, S.; Paillard, E.; Schonhoff, M.; Winter, M.; Passerini, S., New Insights to Self-Aggregation in Ionic Liquid Electrolytes for High-Energy Electrochemical Devices. *Adv. Energy Mater.* **2011,** *1*, 274-281.

39. Castriota, M.; Caruso, T.; Agostino, R. G.; Cazzanelli, E.; Henderson, W. A.; Passerini, S., Raman Investigation of the Ionic Liquid N-Methyl-N-propylpyrrolidinium Bis(trifluoromethanesulfonyl)imide and Its Mixture with $LiN(SO_2CF_3)_2$. *J. Phys. Chem. A* **2005,** *109*, 92-96.

40. Pavlovic, V. P.; Tosic, D.; Dojcilovic, R.; Dudic, D.; Dramicanin, M. D.; Medic, M.; McPherson, M. M.; Pavlovic, V. B.; Vlahovic, B.; Djokovic, V., PVDF-HFP/NKBT composite dielectrics: Perovskite particles induce the appearance of an additional dielectric relaxation process in ferroelectric polymer matrix. *Polymer Testing* **2021,** *96*, 107093.

41. Malzer, T.; Mathies, L.; Band, T.; Gorgas, R.; Leipner, H. S., Influence of Different Solvents and High-Electric-Field Cycling on Morphology and Ferroelectric Behavior of Poly(Vinylidene Fluoride-Hexafluropropylene) Films. *Materials* **2021,** *14*, 3884.

42. Constantino, C. J. L.; Job, A. E.; Simoes, R. D.; Giacometti, J. A.; Zucolotto, V.; Oliveira, O. N.; Gozzi, G.; Chinaglia, D. L., Phase Transition in Poly(vinylidene fluoride) Investigated with Micro-Raman Spectroscopy. *Appl. Spectrosc.* **2005**.

43. Goutev, N.; Ohno, K.; Matsuura, H., Raman Spectroscopic Study on the Conformation of 1,2-Dimethoxyethane in the Liquid Phase and in Aqueous Solutions. *J. Phys. Chem. A* **2000,** *104*, 9226-9232.

44. Mishra, R.; Singh, S. K.; Gupta, H.; Tiwari, R. K.; Meghnani, D.; Patel, A.; Tiwari, A.; Tiwari, V. K.; Singh, R. K., Polar β-Phase PVDF-HFP-Based Freestanding and Flexible Gel Polymer Electrolyte for Better Cycling Stability in a Na Battery. *Energy Fuels* **2021,** *35*, 15153-15165.

45. Hwang, C.; Song, W.-J.; Song, G.; Wu, Y.; Lee, S.; Son, H. B.; Kim, J.; Liu, N.; Park, S.; Song, H.-K., A Three-Dimensional Nano-web Scaffold of Ferroelectric Beta-PVDF Fibers for Lithium Metal Plating and Stripping. *ACS Appl. Mater. Interfaces* **2020,** *12*, 29235-29241.

46. Xing, C.; Zhao, L.; You, J.; Dong, W.; Cao, X.; Li, Y., Impact of Ionic Liquid-Modified Multiwalled Carbon Nanotubes on the Crystallization Behavior of Poly(vinylidene fluoride). *J. Phys. Chem. B* **2012,** *116*, 8312-8320.

47. Huang, M.-M.; Jiang, Y.; Sasisanker, P.; Driver, G. W.; Weingartner, H., Static Relative Dielectric Permittivities of Ionic Liquids at 25 ^{0}C. *J. Chem. Eng. Data* **2011,** *56*, 1494-1499.

48. Rajbangshi, J.; Banerjee, S.; Ghorai, P. K.; Biswas, R., Cosolvent polarity dependence of solution structure in [BMIM][PF_6] + acetonitrile/1,4-dioxane/hexane binary mixtures: Insights from composition dependent Voronoi polyhedra analyses, iso-surfaces and radial distribution functions. *J. Mol. Liq.* **2020,** *317*, 113746.

49. Adams, B. D.; Zheng, J.; Ren, X.; Xu, W.; Zhang, J.-G., Accurate Determination of Coulombic Efficiency for Lithium Metal Anodes and Lithium Metal Batteries. *Adv. Energy Mater.* **2017,** *8*, 1702097.

50. Kol, R.; De Somer, T.; D'hooge, D. R.; Knappich, F.; Ragaert, K.; Achilias, D. S.; De Meester, S., State-Of-The-Art Quantification of Polymer Solution Viscosity for Plastic Waste Recycling. *ChemSusChem.* **2021,** *14*, 4071-4102.

51. Shen, B. H.; Veith, G. M.; Tenhaeff, W. E.; Sacci, R. L., Predictive Design of Shear-Thickening Electrolytes for Safety Considerations. *J. Electrochem. Soc.* **2017,** *164*, A1-A5.

For Table of Contents Only